Measurement and Analysis of Wireless Channel Impairments in DSRC Vehicular Communications

Ian Nathaniel Lim Tan
Wanbin Tang
Ken Laberteaux
Ahmad Bahai

Electrical Engineering and Computer Sciences
University of California at Berkeley

Acknowledgement

Measurement and Analysis of Wireless Channel Impairments in DSRC Vehicular Communications

Ian Tan*, Wanbin Tang†, Ken Laberteaux‡, and Ahmad Bahai*
* Department of Electrical Engineering and Computer Sciences
University of California, Berkeley, CA 94720
{iantan, bahai}@eecs.berkeley.edu
†National Key Laboratory of Communication
University of Electronic Science & Technology of China, Chengdu, China
wbtang@uestc.edu.cn
‡Toyota Technical Center
Ann Arbor, MI 48105
ken.laberteaux@tema.toyota.com

Abstract—We present a GPS-enabled channel sounding platform for measuring both vehicle-to-vehicle and vehicle-to-roadside wireless channels. This platform was used to conduct an extensive field measurement campaign involving vehicular wireless channels across a wide variety of speeds and line-of-sight conditions. From the data, we present statistical characterizations of several classes of these channels at 5.9 GHz. This analysis suggests that while the proposed DSRC standard may account for Doppler and delay spreads in vehicular channels, large packets may face higher error rates due to time-varying channels.

I. INTRODUCTION

The Federal Communications Commission (FCC) has mandated that the frequency spectrum between 5.850 and 5.925 GHz be allocated for dedicated short-range communications (DSRC) in vehicular environments. As a semi-licensed band, this allocation provides an ideal opportunity for automakers, government agencies, commercial entities, and motorists to work in concert to increase highway safety and provide transportation-related services; however, realizing this vision requires reliable, low-latency, wireless communication methods.

The vehicular environment presents a number of challenges that must be understood and appropriately managed in order to enable reliable wireless communications. One core issue is understanding the nature of the wireless channel encountered by vehicular radios. DSRC, once fully deployed, will be used in urban, suburban, and highway environments at a variety of speeds. This alone implies that any communication method employed in the DSRC band will face channels with different delay and Doppler spreads. Knowledge of how these statistics vary with location and speed is essential to designing a DSRC-band communication scheme.

II. PREVIOUS WORK

Previous measurement-based research has included packet level tests that were used to examine the performance of 802.11a in outdoor and mobile situations [1], [2]. However, because fundamental characteristics of the physical channel were not explored, it is difficult to extend their conclusions directly to DSRC performance. Other research included a thorough examination of path loss in [3] and [4] but neither addressed multipath and Doppler effects. Extensive measurement and modeling for channel emulators at 5.9 GHz has been shown in [5]. While providing a modeling technique and an in-depth analysis of a particular expressway location, it does not span a diverse range of possible environments. The measurements in [6]–[8] give time and frequency information in urban and suburban scenarios, but they either neglect extreme Doppler in highway situations (i.e. [6], [7]) or do not investigate non-line-of-sight (NLOS) situations with buildings or trucks as blockers [8]. In addition, the previous works in [3]–[8] do not interpret channel characteristics and their effect upon the DSRC standard.

This work presents the results of physical layer channel measurements and the methods used to obtain them. Measurements are taken over multiple locations spanning a broad spectrum of environments including urban, rural, and highway locales. They also incorporate a variety of speeds with variable line-of-sight (LOS) or non-LOS (NLOS) conditions. In total, over 50 GB of data was collected at over 200 locations. We comment on the implications of the results and consider how they will affect DSRC communications.

III. RELEVANT CHANNEL METRICS

Currently, the IEEE standard proposed for DSRC, known as 802.11p, is based upon the IEEE 802.11a standard. Like 802.11a, 802.11p leverages OFDM to compensate for both time and frequency-selective fading since OFDM copes exceptionally well with the dispersive linear channels found in mobile environments.

One major impairment present in wireless channels is multipath, which corrupts the desired signal with time-delayed and distorted copies. To combat this, a guard interval (or cyclic prefix) is prepended to the beginning of each time-domain symbol. This interval prevents intersymbol-interference (ISI)

between consecutive OFDM symbols, provided that the typical delay spread of the channel is less than the guard interval.

In the frequency domain, broadband signals can suffer from variations across the band in the form of frequency-selective fading. To compensate for frequency-selective fading, OFDM-based systems modulate data on multiple subcarriers. Each subcarrier is allocated a bandwidth, equal to the spacing between subcarriers, that is assumed to behave like a flat fading channel. In a non-mobile environment, subcarriers are naturally orthogonal as each occupies different frequency bands. However, mobility induces Doppler spread, which may cause one carrier to "bleed" information into another. This phenomenon is known as inter-carrier interference (ICI). Ideally, subcarrier spacing is large enough such that any expected Doppler spread is much smaller than this spacing.

Finally, because the vehicular environment changes rapidly with respect to speed, location, and signal scatters, channel characteristics are not static. To quantify this, coherence time is defined as the period of time that a channel may be assumed time-invariant, and it is inversely related to a channel's Doppler spread. Although an OFDM system may be designed with a sufficiently large subcarrier spacing, short coherence times (compared to packet length) can induce errors since the equalization performed at the beginning of a packet's reception does not adapt to channel variations over the reception time.

The signal integrity structures for 802.11a have been optimized for use in indoor situations with slow-moving radios. However, vehicular environments involve severe multipath, higher velocities, and a wider dynamic range of signal strengths. Other than the channel bandwidth and transmission power limits, 802.11p shares the same structure, modulation, and training sequences of the 802.11a PHY. Since the DSRC channel bandwidth is 10 MHz (compared to 20 MHz in 802.11a), this alters parameters directly affecting its ability to cope with multipath, such as symbol guard intervals and subcarrier spacing. Additionally, highway velocities may change the coherence time associated with the channel.

In the remainder of this paper, we describe the means by which we measure the channel, extract relevant parameters, and analyze the suitability of 802.11p for DSRC based on the aforementioned metrics.

IV. CHANNEL SOUNDING SYSTEM

The following subsections detail both the algorithms and specific hardware used for obtaining and analyzing our measurements.

A. Hardware System

As illustrated in Figures 1 and 2, the channel sounding system consists of a transmitter and receiver installed into separate vehicles. The transmitter consists of a laptop, differential GPS (DGPS) unit, Aeroflex 3416 signal generator, high power amplifier, and a 0 dBi MA-COM roof-mounted, omni-directiona antenna. It transmits a channel sounding waveform consisting of a maximal-length, pseudorandom (MLS) $\{\pm1\}$ bit sequence pre-generated in Matlab and modulated via BPSK. The MLS

is 511 bits in length, providing 54 dB of dynamic range, and is generated at a rate of 11 MHz. In the waveform, the data sequence is followed by a 511-bit null period and repeated as shown in Figure 3. Following filtering with a root-raised cosine filter, the 3 dB bandwidth of the transmitted signal is approximately 11 MHz and centered at 5.860 GHz (channel 172). The signals were transmitted at 33 dBm as measured at the antenna input.

The receiver consists of a laptop, differential GPS unit, Litepoint IQView vector signal analyzer (VSA), low noise amplifier for improved sensitivity, and a roof mounted MA-COM antenna. The Litepoint IQView digitizes the downconverted signal and records the data onto the receiver laptop. With the available memory on the Litepoint unit, we receive approximately 15 ms of contiguous data (sampled I and Q) in every data capture. Each data capture is read into a separate file, hereafter referred to as a *superframe*. With the waveform structure described earlier, each superframe contains about 160 *frames*, where we define a frame as a single instance of the MLS and its subsequent null period.

The DGPS units record location information on both laptops with sub-meter accuracy when differential corrections are available. We cross-link transmitter and receiver logs offline to provide an accurate measurement of vehicle locations and velocities for each superframe.
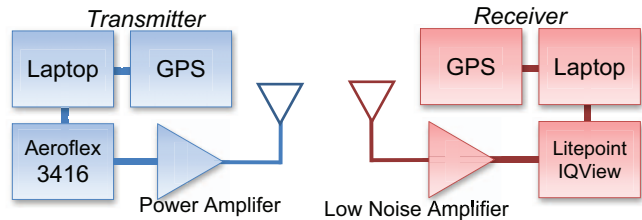

Fig. 1.   Channel sounding architecture.

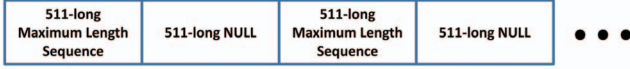Fig. 2.   Channel sounding transmitter vehicular setup.

Fig. 3. Probe waveform.

After the transmitted probe waveform is captured, we post-process it in Matlab with a matched filter algorithm. This generates the spacing and strength of the taps in the multipath model, as well as Doppler, Ricean K-factor, and signal-to-noise ratio (SNR) parameters. The following section provides an overview of the methods used to generate these statistics.

B. Methodology

The instantaneous radio channel can be represented by K multipath delay taps using a finite impulse response (FIR) channel model [9],

$$ h(\tau, t) = \sum_{i=0}^{K-1} A_i(t)\delta(\tau - \tau_i(t)), \qquad (1) $$

where $A_i(t)$ and $\tau_i(t)$ denote the complex channel tap amplitudes and delays at some time t, and $\delta(\tau)$ is Dirac's delta function. In general, this model is linear but time-varying, which is required in order to draw conclusions about Doppler characteristics. If the assumption is made that the channel is linear and time-invariant, the model decomposes into

$$ h(\tau) = \sum_{i=0}^{K-1} A_i\delta(\tau - \tau_i). \qquad (2) $$

We choose to estimate the impulse response of the channel and derive time-varying components (e.g. Doppler spreads) via successive channel estimates. Within a received superframe, each frame is processed individually to produce a single estimate of the channel's impulse response (CIR). These CIR estimates are compiled into a matrix with the delay parameter τ across the columns and each CIR estimate occupying a single row. Since we operate in discrete time, each value of τ is a multiple of our chipping period $T_c = 1/(11 \times 10^6)$. Thus, a typical superframe will generate a CIR matrix of dimension 160 x 511.

To extract a FIR model from each CIR estimate, we utilize a matched filter method detailed in [10], which is a variation of the swept time-delay cross-correlator (STDCC) first used by Cox in [11]. It relies on the impulse-like time-domain cross-correlation properties of MLS sequences, namely that for some periodic MLS sequence $x[n]$ of length and period N,

$$ R_x[k] = \frac{1}{N} \sum_{n=-\infty}^{+\infty} x[n]x[n-k] \qquad (3) $$

is a N-periodic signal which resembles an impulse train, as illustrated in Figure 4.

To calculate the effects of vehicular speed on the wireless channel, we extract the Doppler spectrum for each estimated
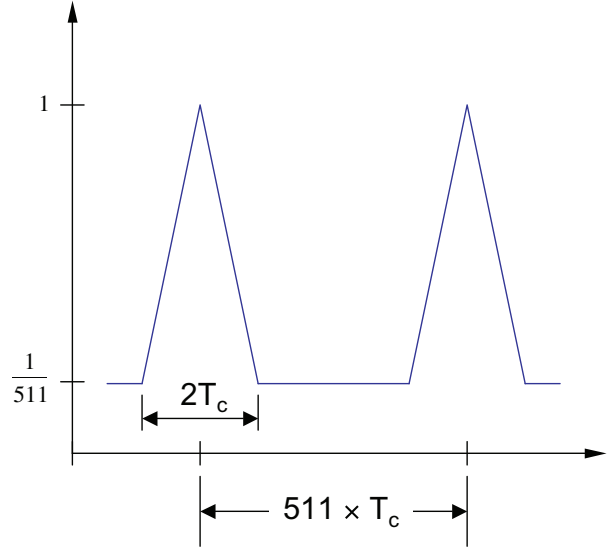

Fig. 4. Plot of the periodic autocorrelation function R_x.

channel tap by taking a windowed FFT down the columns of the CIR matrix,

$$ D(n) = \frac{1}{M} \sum_{k=0}^{M-1} h(n, k)W(k)e^{-2\pi kn/M}, \qquad (4) $$

where $h(n, k)$ is the element in the nth row and k^{th} column of the CIR matrix. The Hamming window function $W(k)$ is

$$ W(k) = 1 - \left(\frac{k - \frac{M-1}{2}}{\frac{M+1}{2}} \right). \qquad (5) $$

Because the total length of each frame is 102.2 μs, consecutive frames produce a repetition rate of 9.8 KHz, yielding a maximum unambiguous Doppler frequency of ±4.9 KHz.

In situations where a line-of-sight (LOS) path is present, knowing the relative strengths of the dominant LOS path to other paths assists in quantifying the degree of determinism in the channel. We calculate this statistic, known as the Ricean K-factor, for each tap via the moment-method [12].

V. MEASUREMENT SCENARIOS

Using the system detailed in Section IV, we conducted an extensive channel measurement campaign in and around Detroit, Michigan. We investigated an open-field test track, streets in urban canyons, rural roads, and highways with mixed traffic. These situations provided channel measurements with varying scatter densities, speeds, and LOS conditions. By examining many channels with varying realizations of these parameters, the suitability of the proposed DSRC standard to real wireless vehicular channels could be assessed.

The first type of environment involved an automotive proving ground. It consisted of a straight, four-lane asphalt test track situated in an open field. We conducted tests that

replicated conditions for roadside-to-vehicle and oncoming vehicle-to-vehicle situations. Other tests measured path loss along the track. This provided a controlled, uncluttered environment with few multipath sources, which yielded baseline measurements for our system.

The second type of environment consisted of the downtown streets in a major metropolitan area. We tested at a number of streets in Detroit that were flanked by large, multi-story buildings. For the primary LOS case, two vehicles approached each other at approximately 30 mph from either end of an urban canyon 800 m in length. To collect NLOS data, we used a four-way intersection with buildings on three corners. A stationary vehicle was placed about 50 m from the intersection, while the second vehicle would approach the intersection from a cross street.

The third type of environment involved several interstate highways. Tests were conducted on two-way multi-lane roads at speeds over 50 mph with separations ranging from 100 m to 1000 m. The surrounding environment varied greatly due to presence of hills, overpasses, and other concrete structures. Traffic was also uncontrolled with a mix of passenger vehicles and large tractor trailer trucks. NLOS conditions were created either by terrain or by the imposition of blocking vehicles (usually large trucks) between our transmitter and receiver.

VI. RESULTS AND ANALYSIS

A. Parameter Extraction

From the environments previously described, we first compiled statistical descriptions of channels at each measurement location. Locations were then categorized into scenarios by locale, vehicle separation, and LOS/NLOS conditions (where applicable).

For each CIR matrix, a power delay profile (PDP) was calculated for each row as

$$P(n, \nu) = \sum_{k=0}^{510} |h(n, k)|^2 \delta(\nu - k), \quad (6)$$

where n is the row index, ν is a discrete delay index, and $h(n, k)$ is as defined in (4). Each PDP was also normalized to the strength of the strongest tap. Next, an average PDP was computed for each superframe by averaging all the normalized PDPs in the superframe's CIR matrix. A 30 dB threshold, relative to the strongest tap, was then applied to remove weak taps and spurious responses due to system noise.

To summarize the delay spread characteristics of each scenario, the mean excess delay, RMS delay, and max excess delay were calculated for each averaged PDP. They were then averaged across the superframes for a given scenario with the corresponding results given in Table I. For our measurements, max excess delay is defined as the delay value of the latest tap which is no more than 30 dB below the strongest tap. Mean excess and RMS delay are defined as the first moment and second central moment, respectively, of the average PDP [13]. The relationship between delay spread parameters is shown in Figure 5.
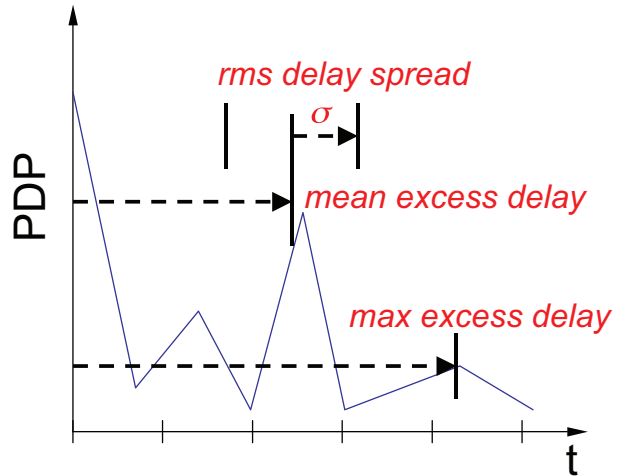

Fig. 5. Relationship between delay parameters.

One example of an average PDP derived from an Urban LOS measurement is shown in Figure 6. Notice the strong initial tap at 250 ns, followed by a number of weaker reflections until approximately 3100 ns. The plot indicates that although the LOS path dominates, a number of significant reflections are still present and contribute to a large RMS delay spread of 501.8 ns. Contrast this with the Highway LOS PDP shown in Figure 7. Due to a reduced scatterer density, this PDP has significantly fewer taps, a faster decay rate, and a smaller RMS delay spread of 191.3 ns.
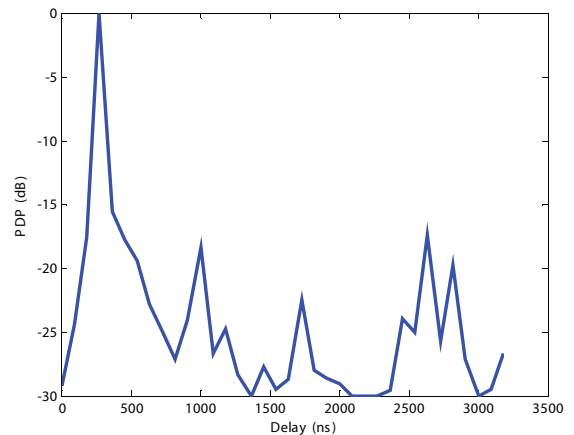

Fig. 6. PDP of an Urban LOS channel.

Each of the taps of the PDP will possess an associated Doppler spread, which is calculated from the spectrum determined in (4). Figure 8 shows a sample Doppler plot for the fourth tap in a Highway LOS case. The Doppler spread is calculated as the support of the spectrum, which is approximately 2 KHz. Doppler shift is calculated as $0.5 * (f_{max} + f_{min})$, where f_{max} and f_{min} are the upper and lower bounds of the Doppler spectrum's support, respectively. Highway speeds for our tests were about 30 m/s, and the waveform carrier
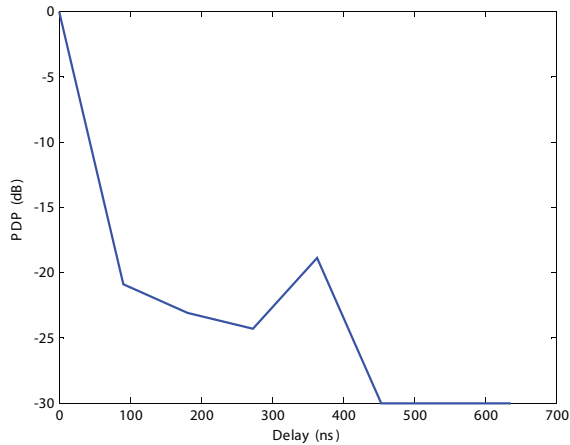
Fig. 7.   PDP of a Highway LOS channel.

frequency was 5860 MHz. Thus, Doppler shifts of 1.1 KHz or higher are possible when reflections off obstructions directly ahead of the transmitter and receiver are considered. For example, a reflection off an overpass gives an effective path closure rate of 60 m/s and a Doppler shift of 1172 Hz. Reflections off approaching vehicles (also traveling at 30 m/s) lead to a closure rate of 120 m/s and a Doppler shift of 2.3 KHz. Since the Doppler spread accounts for a range of reflections from many angles (and hence different closure rates), a spread of 2 KHz is not unreasonable. A closer examination of the spectrum's shape indicates a strong component at 0 Hz, which suggests that a paths orthogonal to the receiver vehicle's line of motion contribute strongly to this tap. Aside from the DC component, the spectrum resembles the "bathtub" shape typical of a Rayleigh-faded tap.
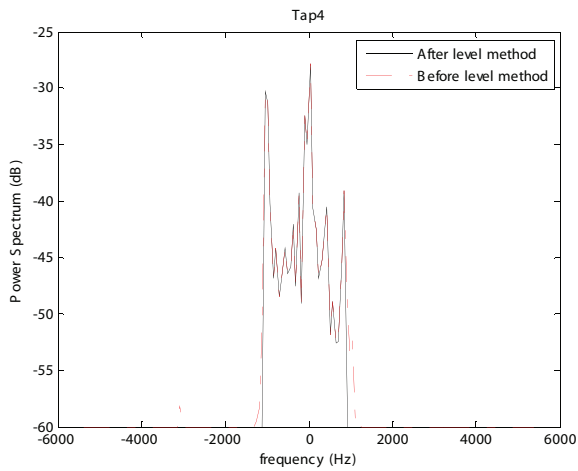

Fig. 8.   Doppler spectrum of the fourth tap of a Highway LOS channel.

Compared to other work, our measurements encompass a variety of different locations which we classify into scenarios via measurement locale (urban, suburban, etc.), line-of-sight conditions, and receiver-transmitter (RX-TX) separation.

Although it is possible to analyze each location separately, understanding the channel impairments, on average, for each scenario is more valuable for determining the expected performance of 802.11p. Table I summarizes the statistical data for a selection of the scenarios available. For a set of superframes in a given scenario, delay parameters are calculated by averaging over all superframes, while frequency and Doppler parameters are averaged over all taps within the set of superframes.

B. Analysis

Looking first at the Urban LOS/NLOS scenarios, we note that Doppler spreads are similar in magnitude between the LOS and NLOS cases and that they correspond to urban speeds (30-35 mph). However, the Urban NLOS delay spread (mean, RMS, and max excess) is noticeably larger than that of the Urban LOS case at an equivalent RX-TX separation. This is accounted for by the increased number of reflections, as well as signal attenuation, that are incurred in NLOS scenarios.

Among the high speed scenarios (Highway LOS/NLOS and Rural), it is apparent that the Rural environment is the least hostile among the three due to its small delay spreads resulting from a lack of scatters. On the other hand, the Highway NLOS scenario at 400 m is the most hazardous out of all the cases tested. All its delay parameters and its average Doppler spread exceed that of any other case. Since large trucks were used to create NLOS conditions, it is likely that metal trailers were responsible for creating a rich multipath environment. The Doppler spread, while high, can be attributed to increased vehicular speeds, as all Highway and Rural scenarios have Doppler spreads on the same order of magnitude. We also note that, from a safety perspective, the Highway NLOS environment is one that would benefit significantly from DSRC assistance due to the combination of high speeds and reduced driver reaction time.

An examination of Table I in light of the metrics mentioned in Section III suggests that the proposed design parameters of 802.11p should account for most of the channel impairments. We start by comparing the guard interval with the delay spreads to determine the degree to which multipath will introduce ISI. For 802.11p, this guard interval (GI) is 1.6 μs, which is twice as long as 802.11a's GI of 0.8 μs. To quantify delay spread, we examine the sum of mean excess delay and RMS delay, as opposed to examining each individually. This is a reasonable metric as RMS delay measures the spread of delays about the mean excess delay, so their sum gives a statistical measure of the delay spread starting from the beginning of the PDP. We refer to this metric as the *sum delay spread*.

Although many max delay spreads are over the 1.6 μs interval, the sum delay spreads across all scenarios lie below the 1.6 μs guard interval. This implies that ISI should not be a significant problem. Taps contributing to the max delay will always cause a slight amount of interference, but their magnitude (around 30 dB below the strongest tap) should not be great enough to impact performance significantly.

TABLE I
STATISTICAL RESULTS BY SCENARIO

Locale	Distance (m)	Delay Parameters (ns)			Frequency Parameters (Hz)	
		Mean Excess	RMS	Max Excess (30 dB)	Frequency Shift	Avg. Doppler Spread
Rural LOS	100	85.8	21.6	272.7	201	782
Urban LOS	200	303.2	157.5	1681.8	-20	341
	400	370.1	320.6	3781.8	203	263
	600	515.9	286.6	3625	-21	294
Urban NLOS	200	521.7	295	2454.5	103	298
Highway LOS	300	154.1	156.8	2026	209	761
	400	175.4	141.1	1575.8	261	895
Highway NLOS	400	558.5	398	4772.7	-176	978

As stated in Section III, high Doppler spreads may cause ICI between OFDM subcarriers. However, from the table we see that average Doppler spreads are, at most, 978 Hz. This is a small fraction of the 156.25 KHz inter-carrier spacing for 802.11p. In fact, it was rare to see a channel tap with a Doppler spread over 2 KHz, which is still only 1.28% of the intercarrier spacing. Hence, even under the most hazardous Doppler conditions, the amount of ICI should be minimal.

Therefore, based solely on Doppler and delay metrics, the standard should be capable of reasonable performance, although improvements can be made and certain issues still remain. For example, although the reported Doppler spreads may not cause significant ICI, the coherence times they induce may cause problems for longer packets. The relation of Doppler spread D_s to coherence time is given as

$$T_{coh} = \frac{M}{D_s}, \tag{7}$$

where the constant M varies anywhere from 0.25 to 1 [9], [13]. Correspondingly, a Doppler spread of 978 Hz gives a coherence time anywhere between 0.26 ms to 1.02 ms. For short packets, the channel may remain relatively invariant over the course of the packet. However, longer packets may experience more fluctuations in the channel which are not compensated for by initial equalization settings.

Figure 9 illustrates the relationship among coherence time, PHY payload size, and rate. Assuming an upper estimate of T_{coh} = 1.02 ms and a transmission rate of 3 Mbps, it is likely that any packets over 367 bytes will experience multiple channel fades. Moving to higher-order modulations will increase the probability of having an invariant channel but risks increased sensitivity to Doppler and ICI. Furthermore, if the lower estimate of T_{coh} = 0.26 ms applies, then even at 24 Mbps packets over 660 bytes will likely experience multiple fades.

The acting ASTM DSRC standard [14] states that compliant devices must sustain a PER < 10% when traveling at 85 mph and sending 1000 byte packets *and* when traveling at 120 mph and sending 64 byte packets. Based on these two speeds, the maximum average Doppler spread of 978 Hz, and a typical Highway NLOS speed of 66.5 mph, we estimate the coherence times for these two cases and plot their relationship to transmission times in Figure 10. From the figure, we see that 1000 byte packets at 85 mph will likely suffer from multiple

channel fades at several data rates unless improvements, such as multiple equalizations over a packet transmission, are made.
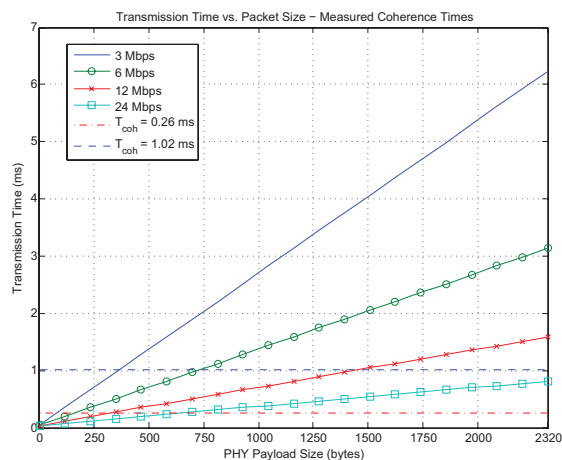

Fig. 9. Plot of transmission time for various rates and payload sizes. Upper and lower bounds to the coherence time are superimposed.
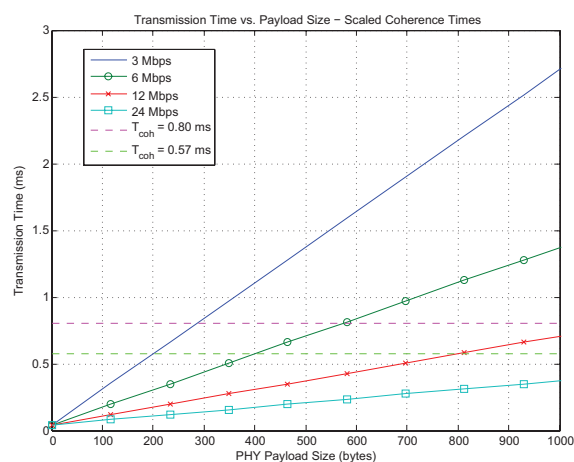

Fig. 10. Same display as Figure 9, but with coherence times scaled for 85 and 120 mph speeds.

VII. CONCLUSION

After conducting a field measurement campaign across more than 200 locations, we have collected in excess of 50 GB of data and used it to perform large-scale characterization of many vehicular wireless channels. These characterizations have shown that, in general, the proposed DSRC standard compensates appropriately for increased delay and Doppler spreads present in such channels. However, the analysis also suggests that channel invariance over large packets (over 367 bytes) cannot be assumed. Consequently, although the proposed standard may perform acceptably for short transmissions, longer transmissions may be subject to higher error rates in the absence of further processing.

ACKNOWLEDGMENTS

REFERENCES

[1] I. Bradaric, R. Dattani, A. Petropulu, J. Schurgot, F.L., and J. Inserra, "Analysis of physical layer performance of IEEE 802.11a in an ad-hoc network environment," in *Proc. IEEE Military Communications Conference (MILCOM'03)*, vol. 2, Oct. 13–16 2003, pp. 1231–1236.

[2] S. Sibecas, C. Corral, S. Emami, and G. Stratis, "On the suitability of 802.11a/RA for high-mobility DSRC," in *Proc. 55th IEEE Vehicular Technology Conference (VTC Spring '02)*, vol. 1, May 6–9 2002, pp. 229–234.

[3] T. Schwengler and M. Gilbert, "Propagation models at 5.8 GHz – path loss and building penetration," in *Proc. IEEE Radio and Wireless Conference (RAWCON 2000)*, Sep. 10–13 2000, pp. 119–124.

[4] G. Durgin, T. Rappaport, and H. Xu, "Measurements and models for radio path loss and penetration loss in and around homes and trees at 5.85 GHz," *IEEE Trans. Commun.*, vol. 46, no. 11, pp. 1484–1496, Nov. 1998.

[5] G. Acosta and M. Ingram, "Doubly selective vehicle-to-vehicle channel measurements and modeling at 5.9 GHz," in *Proc. Wireless Personal Multimedia Communications Conference (WPMCC'06)*, Sep. 2006.

[6] X. Zhao, J. Kivinen, P. Vainikainen, and K. Skog, "Propagation characteristics for wideband outdoor mobile communications at 5.3 GHz," *IEEE J. Sel. Areas Commun.*, vol. 20, no. 3, pp. 507–514, Apr. 2002.

[7] ——, "Characterization of Doppler spectra for mobile communications at 5.3 GHz," *IEEE Trans. Veh. Technol.*, vol. 52, no. 1, pp. 14–23, Jan. 2003.

[8] D. Matolak, I. Sen, W. Xiong, and N. Yaskoff, "5 GHz wireless channel characterization for vehicle to vehicle communications," in *Proc. IEEE Military Communications Conference (MILCOM'05)*, vol. 5, Oct. 17–20 2005, pp. 3016–3022.

[9] D. Tse and P. Viswanath, *Fundamentals of Wireless Communication*, 1st ed. New York, NY: Cambridge Univ. Press, 2005.

[10] G. Acosta-Marum, "Measurement, modeling, and OFDM synchronization for the wideband mobile-to-mobile channel," Ph.D. dissertation, Geogia Institute of Technology, May 2007.

[11] D. Cox, "Delay Doppler characteristics of multipath propagation at 910 MHz in a suburban mobile radio environment," *IEEE Trans. Antennas Propag.*, vol. 20, no. 5, pp. 625–635, Sep. 1972.

[12] L. Greenstein, D. Michelson, and V. Erceg, "Moment-method estimation of the Ricean K-factor," *IEEE Commun. Lett.*, vol. 3, no. 6, pp. 175–176, Jun. 1999.

[13] T. Rappaport, *Wireless Communications: Principles and Practice*, 2nd ed. Prentice Hall, 2002.

[14] *Standard Specification for Telecommunications and Information Exchange Between Roadside and Vehicle Systems – 5 GHz Band Dedicated Short Range Communications (DSRC) Medium Access Control (MAC) and Physical Layer (PHY) Specifications*, ASTM Std. E2213-03, 2003. [Online]. Available: www.astm.org